Proceedings Paper:
Almshahy, A., Al Qubeissi, M., Al-Damook, M. et al. (2 more authors) (Accepted: 2025) Investigating the Effect of Hydrogen-Helium Blends on Thermal Management Efficiency in Battery Systems. In: AIP Conference Proceedings. The 7th Scientific Conference for Postgraduate Engineering Research (SCPER2025), 03-04 Dec 2025, Baghdad, Iraq. American Institute of Physics. ISSN: 0094-243X. EISSN: UNSPECIFIED. (In Press)

Investigating the Effect of Hydrogen-Helium Blends on Thermal Management Efficiency in Battery Systems

Ali Almshahy,[1,2, a)] Mansour Al Qubeissi,[3, b)] Moustafa Al-Damook,[4, c)] Zinedine Khatir,[1, d)] K. J. Kubiak,[1, e)]

[1] *School of Mechanical Engineering, Faculty of Engineering and Physical Sciences, University of Leeds, LS2 9JT, UK.*
[2] *Inspection and Asset Integrity Department, Zubair Field Operating Division, Basra Oil Company (BOC), Ministry of Oil, Basra 240, Iraq.*
[3] *College of Engineering Technology, University of Doha for Science and Technology, Doha 24449, Qatar.*
[4] *Department of Quality Assurance and Academic Accreditation, University of Fallujah, Fallujah 31002, Iraq*

[a)] *Corresponding Author:* Fsvl1319@Leeds.ac.uk
[b)] Mansour.alqubeissi@udst.edu.qa
[c)] Moustafa.al-damook@uofallujah.edu.iq
[d)] Z.Khatir@Leeds.ac.uk
[e)] K.Kubiak@Leeds.ac.uk

Abstract. An effective battery thermal management system (BTMS) is crucial for ensuring the safety, longevity, and performance of lithium-ion batteries (LIB) in electric vehicles (EVs). This study investigates the performance of BTMS using innovative gas mixtures of hydrogen and helium as coolants. The research focuses on varying concentrations of these gases, with hydrogen to helium ratios ranging from 90:10 to 60:40 in 10% increments of helium. The integration of inert helium with hydrogen mitigates flammability risk and effectively maintains optimal LIB operating conditions. The thermal performance of immersion cooling for a cylindrical LIB cell (4000 mAh) was evaluated using computational fluid dynamics (CFD) software (ANSYS Fluent). Temperature response and power consumption were analysed at a high discharge rate of 2C, with varying coolant inlet velocities (0.5 m/s, 1 m/s, 5 m/s, and 20 m/s) and helium concentrations. A key finding of the study is that higher concentrations of helium led to a trade-off in BTMS performance: while improving safety, thermal performance slightly decreased, and pressure drop increased. These effects are attributed to the increased density of the gas mixture, which heightens frictional losses and flow resistance. Across all test scenarios, the maximum LIB temperature was consistently maintained below the threshold of 40°C. This finding reinforces the effectiveness of the gas mixture strategy in ensuring both safe operation and reliable performance of LIB in EVs.

Keywords: Battery thermal management; Electric vehicle; Cooling performance; Hydrogen, helium, Battery pack.

INTRODUCTION

The escalating global warming crisis and energy shortage demand urgent attention and decisive action. In response, many countries have adopted emission reduction and energy saving plans, aimed at achieving significant decarbonization by 2050 [1]. Statistics indicate that around 30% of greenhouse gases emissions (GHG) are produced from conventional vehicles. As a result, electric vehicle (EV) is a promising solution to mitigate GHG and reduce air pollution [2]. Lithium-ion battery (LIB) is considered the core power of hybrid/pure electric vehicle due to high energy density, less self-discharge, and long-life cycle [3]. However, lifespan, performance, operational safety of LIB are considerably degraded by excessive temperature. Effective battery thermal management systems (BTMS) are essential to ensure operational temperature (20-40 °C), with uniform temperature distribution less than 5°C [4], [5].

Currently, the most common cooling technologies have used thermal management of batteries including air cooling, liquid cooling, and phase change materials (PCMs) [6, 7]. Air cooling offers advantages such as simple design, easy maintenance and lower cost. However, its low heat dissipation poses an inherent limitation in BTMS [8]. The PCM is an effective passive cooling technique that leverages latent heat storage through the charging and discharging process. Whereas, under high load conditions, its ability to regulate battery operating conditions is compromised due to low thermal conductivity [9]. Indirect liquid cooling employs various technologies to effectively remove the battery heat generation, including cold plates, pipes channel, and water jacket. Although it exhibits superior thermal performance, the system design is relatively bulky and complex. Additionally, encounter inhomogeneous

temperatures distributions under stressful conditions due to thermal resistance between the battery surface and metal separator [10].

An innovative and powerful alternative cooling strategy to the BTMS is direct liquid cooling, known as immersion cooling. Immersion cooling systems' impressive thermal performance and preserve even temperature distribution due to the battery in direct contact with dielectric working fluids [11]. This innovative cooling approach significantly enhances efficiency and prolongs components lifespan, making it a superior choice for modern cooling solutions. Recent studies have validated its effectiveness: Haosheng et al. demonstrated that transformer oil and PAO-4 show superior thermal performance even at extensive conditions [12]. While Al Qubeissi et al. illustrated that using fuel as coolants primarily contributes to enhance the cooling efficiency and achieve BTMS lightweight [13]. This highlights the capabilities of immersion cooling systems in dissipating excessive heat generation even under extensive conditions and preventing thermal runway.

Another aspect of suppression thermal runway in batteries uses inert gases such as nitrogen and argon [14]. Boonkit et al. proposed inert gases as an alternative coolant in BTMS to avoid fire propagation and thermal runway. Although all gases kept the battery temperature within the optimal range, helium gas performs exceptionally even at low Reynolds numbers. Another study explored a novel cooling method using hydrogen, conducted by Al-Zareer et al. [15]. This approach uses compressed hydrogen to effectively cool the batteries prior to their injection into the fuel cell, enhancing overall efficiency and performance. Hydrogen is considered the key solutions to combat environmental issues and global warming [16]. However, hydrogen is an extremely flammable gas and possesses a substantially wider flammable range [17]. Thus, the mixture of hydrogen with inert gases such as helium substantially contributes to reducing flammability and enhances the cooling advantage [18].

To the authors' knowledge, no previous study has investigated a BTMS using the proposed hydrogen-helium gas mixtures for EV applications. This work aims to address this research gap by rigorously evaluating the thermal performance and power consumption of the system across a range of helium gas concentrations, from 10 % to 40 % in 10% increments. By employing hydrogen gas as the primary coolant, blended with various concentrations of helium, the approach aims to enhance thermal performance while significantly mitigating the flammability risks. This methodology allows for a thorough evaluation of how different helium concentrations influence BTMS performance, paving the way of advancement in EV technology. The proposed system was analysed numerically using CFD (using ANSYS software tool). The combined electro-thermal model was validated against established experimental and numerical data [19], ensuring the reliability and relevance of our findings.

NUMERICAL MODEL

This section presents the conceptual framework and numerical methodology of using hydrogen-helium gas mixtures for LIB cooling. The following parts will elaborate on the geometric design, the governing equations, the electrochemical-thermal battery model, boundary conditions, and the analysis approach.

Geometry Design

In this study, the battery module comprises $LiFePO_4$ cylindrical batteries arranged in a 5S1P configuration (five cells in series, one in parallel). The specifications and thermophysical properties of the cylindrical cell, tab, and busbar are presented in Tables 1.

TABLE1. Li-ion cylindrical cell specifications

Specification of Cylindrical cell	Value
Nominal cell capacity	4000 mAh
Nominal Voltage	3.2 V
Maximum Voltage	4.3 V
Minimum Voltage	3 V
Cathode type	$LiFePO_4$
Anode type	Graphite

Diameter of the cell	21.3 mm
Height of the cell	70 mm

The thermophysical properties of the battery module's constituent materials are fundamental to understanding its thermal behavior. The lithium-ion cell itself has a density of (2029 kg/m³), a specific heat capacity of (678 J/kg·K), and a relatively axial thermal conductivity of (18.2 W/m·K) [19, 20], which inherently resists the transfer of heat from its core. In contrast, the electrical interconnects are designed for efficient thermal management. The tabs, inferred to be made of aluminum, exhibit a high density of (8978 kg/m³), a specific heat capacity of (381 J/kg·K), and an excellent thermal conductivity of (387.6 W/m·K), enabling them to act as highly effective heat spreaders from the cell terminals. Similarly, the busbar, with properties characteristic of copper (density: 2719 kg/m³, specific heat: (871 J/kg·K), thermal conductivity: (202.4 W/m·K), serves not only as an electrical conductor but also as a crucial component for distributing and dissipating heat throughout the module, thereby compensating for the cell's poor conductivity properties.

The battery module with its enclosure was designed using ANSYS Design-Modeler (V/2024R2). The cooling is based-immersion technology with partially submerged cells to dissipate the heat generated. The nominal cell capacity and voltage of a single cell are 4 Ah and 3.2 V, respectively. The spacing between batteries is set to 6.7 mm. Electrical connections are made using aluminum tabs and copper busbars, as shown in Fig. 1(a). Figure 1(b) shows the cylindrical single cell.

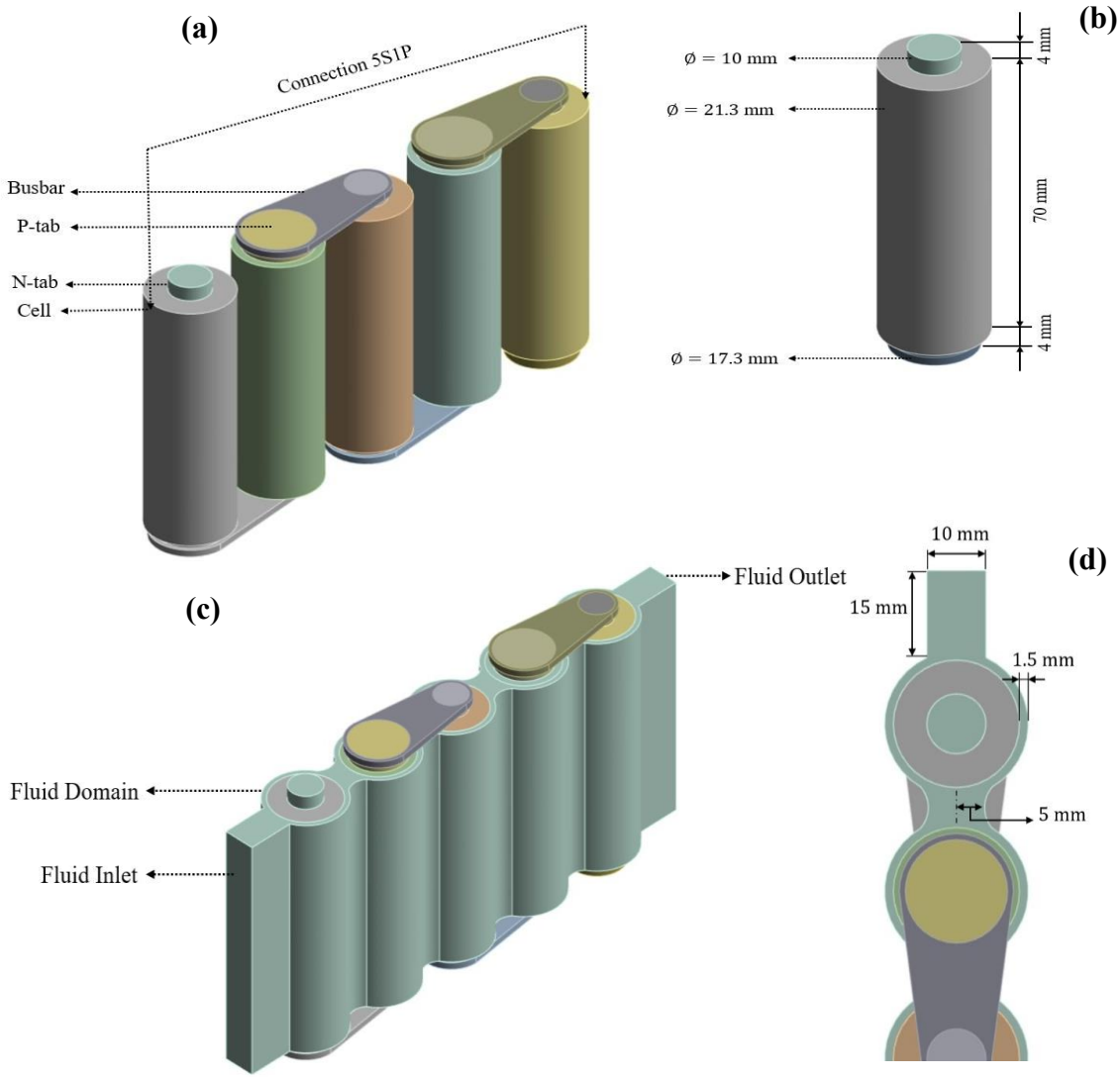

FIGURE 1. Schematic of the battery module (a) 5S1P arrangement, (b) single battery cell, (c) battery module with enclosure, and (d) tope view of enclosure.

As shown in Fig. 1(c) & (d), the battery cells are partially immersed in dielectric working fluids. This innovative enclosure design allows the working fluids to envelop the cells, resulting in improved thermal performance. Additionally, it plays a crucial role in reducing thermal resistance and promoting uniform temperature distribution. The main objective is to regulate the maximum temperature within an optimal range while ensuring an even temperature distribution throughout the system.

NTGK Model

LIB modelling is complex due to its muti-physics and multi-domain nature, involving interactions across various length and time scales [21]. The multi-domain framework used in this study is adept at capturing the intricate interactions among diverse physicochemical processes. The Electrochemical-thermal Model (ECM) is implemented, using the Newman, Tiedeman, Gu, and Kim (NTGK) model [22, 23]. The NTGK model is favored due to its computational efficiency, accuracy in matching experimental data, and effectiveness for numerical simulation of battery cells. To comprehensively understand the electro-thermal coupling of a Li-ion battery, referred to Fig. 2.

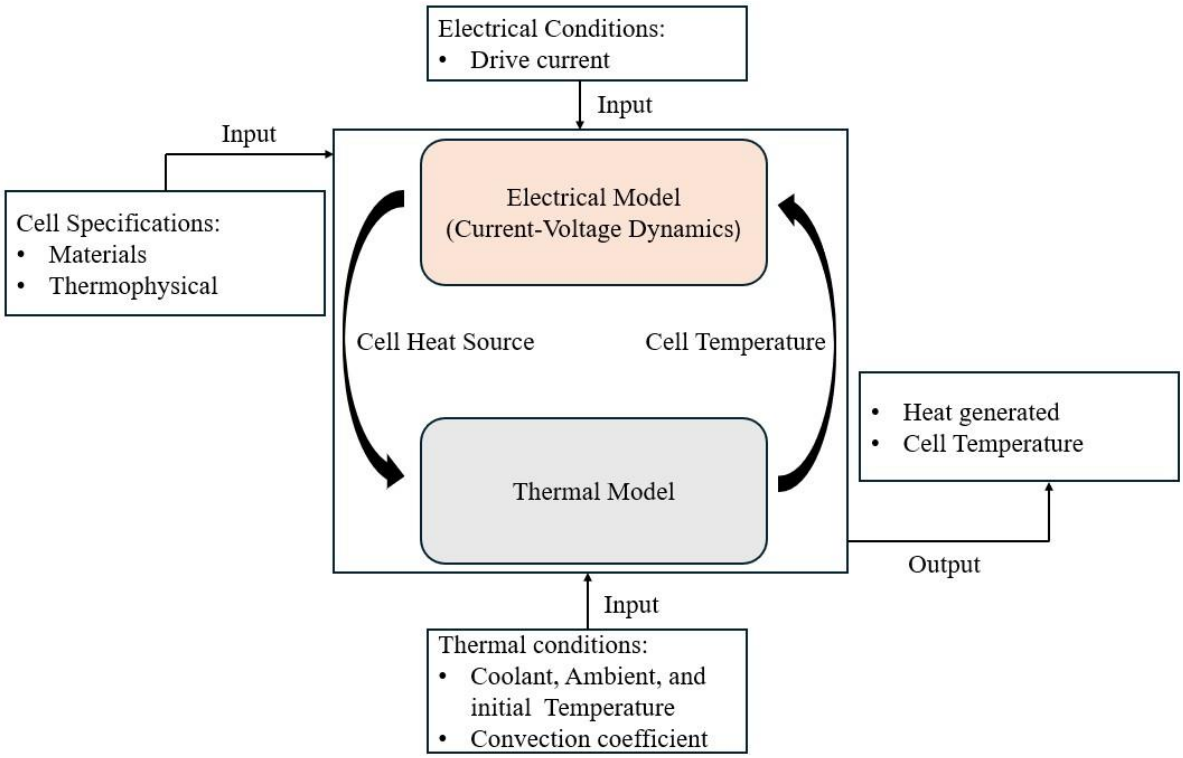

FIGURE 2. Diagram of Electro-Thermal Coupling (ETC) for battery

The electro-thermal fields within a battery are analyzed in the CFD by discretizing the relevant differential equations [23]. Energy conservation of the thermal and electrical for the battery is computed by using equation 1. Governing equations of the current flux at the positive and negative electrode are expressed as [21, 24]:

$$\frac{\partial \rho_b C_{p,b} T}{\partial t} = -\nabla \cdot [k_b \nabla T_b] = \sigma_+ |\nabla \varphi_+|^2 + \sigma_- |\nabla \varphi_-|^2 + \dot{q}_{ECh}, \tag{1}$$

$$\nabla . (\sigma_+ \nabla \varphi_+) = -(j_{ECh} - j_{\text{short}}), \tag{2}$$

$$\nabla . (\sigma_- \nabla \varphi_-) = j_{ECh} - j_{\text{short}}, \tag{3}$$

where, σ_+ and σ_- are positive and negative electrode electrical conductivity, respectively. φ_+ and φ_- are positive and negative electrode phase potential, correspondingly. $T, \rho_b, \ and \ k_b$ represent temperature, density and thermal conductivity, respectively. j_{ECh} and j_{short} represent current transfer due to electro-chemical and internal short circuit, respectively.

The current transfer density (j_{ECh}) and depth of discharge (DOD) are computed as:

$$j_{ECh} = \frac{Q_{\text{nominal}}}{Q_{\text{ref}} Vol_b} Y[U - V], \tag{4}$$

$$\text{DOD} = \frac{Vol_b}{3600 Q_{\text{nominal}}} \int_0^t j \, dt, \tag{5}$$

where, $Q_{nominal}$ is the cell capacity, Q_{ref} is the reference capacity used in the experimental to obtain the depth of discharge which are Y and U.

The heat generated by the electrochemical reaction in the battery is calculated using Equation 6. The first and second terms in this equation represent heat generation due to overpotential and entropic heating, respectively. The parameters Y and U, which indicate the battery's depth of discharge, are determined as:

$$q_{ECh} = J_{ECh} \left[(U - V) - T \frac{dU}{dT} \right], \tag{6}$$

$$U = a_0 + a_1\,(DOD)^1 + a_2(DOD)^2 + a_3(DOD)^3 + a_4(DOD)^4 + a_5(DOD)^5, \quad (7)$$

$$Y = b_0 + a_1\,(DOD)^1 + b_2(DOD)^2 + b_3(DOD)^3 + b_4(DOD)^4 + b_5(DOD)^5. \quad (8)$$

Governing Equation and Boundary Conditions

3D transient heat transfer is established for the battery module and working fluids to numerically evaluate the efficiency of BTMS-based immersion cooling. Battery energy conservation equation is expressed in Equation 1. The governing conservation equations that characterize fluid flow and heat transfer during both heat generation and cooling have been rigorously formulated in Equations 9-13, providing a robust foundation for understanding these critical processes. The continuity, momentum and energy equations for dielectric fluids, respectively, are:

$$\frac{\partial \rho_c}{\partial t} + \nabla . (\mathcal{V}_c . \rho_c) = 0, \quad (9)$$

$$\frac{\partial \rho_c}{\partial t}\mathcal{V}_c + \nabla(\mathcal{V}_c . \rho_c)\mathcal{V}_c = -\nabla p + (\mu_c \nabla \mathcal{V}_c), \quad (10)$$

$$\rho_b\, C_{p,b}\, \frac{\partial T_c}{\partial t} + \nabla . \left(\rho_b\, C_{p,b}\, \mathcal{V}_c\, T_c\right) = \nabla . (K_c\, \nabla\, T_c), \quad (11)$$

where $\rho_c, \mathcal{V}_c, K_c, T_c, \mu_c$ are density, velocity, thermal conductivity, temperature, and dynamic viscosity, respectively.

The K-epsilon ($k - \varepsilon$) realizable model is applicable for gas mixtures in this problem [25]. The equation of $k - \varepsilon$ are expressed as follows:

$$\frac{\partial \rho k}{\partial t} + \nabla * [\rho \vec{V} k] = \nabla * [(\mu + \frac{\mu_t}{\sigma_k})\nabla k] + G_k + G_b - \rho\varepsilon - Y_M + S_k, \quad (12)$$

$$\frac{\partial \rho \varepsilon}{\partial t} + \nabla * [\rho \vec{V} \varepsilon] = \nabla * [(\mu + \frac{\mu_t}{\varepsilon_k})\nabla \varepsilon] + C_1 \frac{\varepsilon}{k}(G_k + C_3 G_b) - C_2 \rho \frac{\varepsilon^2}{k} + S_\varepsilon, \quad (13)$$

where, σ_k and ε_k are kinetic energy and eddy viscosity for turbulent Prandtl numbers, respectively. μ and μ_t are dynamic viscosity and turbulent viscosity for blending gases. G_k and G_b are turbulence kinetic energy due to buoyancy. Y_M is the fluctuation dilatation, respectively. S_k and S_ε are user defined source.

To evaluate the thermal performance and power consumption of BTMS-immersion cooling, maximum temperature, temperature variation and pressure drop are calculated. Temperature variation, pressure drop, and power consumption are expressed as follows [4, 26, 27]:

$$\Delta T(t) = max\{T_i(t)\} - min\{T_i(t)\}, i \in \{1,2,3,4,5\}, \quad (14)$$

$$\Delta P = P_{in} - P_{out}, \quad (15)$$

$$\text{Power} = \Delta P \times A \times \mathcal{V}. \quad (16)$$

Where $\Delta T, \Delta P, \mathcal{V}$, and A are the temperature variation, pressure drop, coolant velocity, and cross section area, respectively.

The governing equations and NTGK model are solved by using ANSYS-Fluent V2024R2. Implicit transient method and pressure passed solver with second-order upwind are employed to solve the thermo-fluid-solid problem. The inlet and outlet conditions are set as velocity and pressure, respectively. The initial and inlet temperature is set at 25°C, while the outlet temperature is atmospheric pressure. The battery module discharge current rate is fixed at 2C-rate. Working fluid velocity is ranged as (0.5m/s, 1m/s, 5m/s, and 20m/s). The flow model is assumed as a turbulent ($k - \varepsilon$) to be applicable with gas mixtures. The outer surface of the enclosure is assumed to be adiabatic. The convergence criteria for the continuity, momentum, and energy equations' residuals are set to 10^{-3}, 10^{-3}, and 10^{-6},

respectively, to ensure the accuracy of the numerical results. A transient thermal model was simulated at 1s time step size and 20 number of iterations until the battery module fully discharged at 2C-rate.

Hydrogen-Helium Gases

Hydrogen is known as a versatile energy carrier, used across power generation, refining, and manufacturing sectors [28], with growing use in automotive fuel cells or internal combustion engines [29]. This widespread adoption hinges on improving system durability, reliability, efficiency, and cost-effectiveness [30, 31]. While hydrogen offers a path to decarbonization, its high flammability necessitates stringent safety measures. Therefore, in this study, hydrogen is blended with helium at various concentrations that substantially contribute to reducing flammability by increasing the ignition threshold. Additionally, it evaluated the thermal performance of system at different hydrogen-helium concentrations. Table 2 shows the thermo-physical properties of gases.

TABLE 2. thermo-physical properties of gases

Fluid	State	Density ($Kg.m^{-3}$)	Specific heat ($J.Kg^{-1}.K^{-1}$)	Thermal conductivity ($W.m^{-1}.K^{-1}$)	Viscosity ($Kg.m^{-1}.s^{-1}$)
Hydrogen	Gas	0.08189	14283	0.1672	0.000008411
Helium	Gas	0.1625	5193	0.152	0.0000199

Choosing the appropriate working fluid significantly impacts its thermal performance. Numerous working fluids are available within the required temperature range, and various characteristics must be evaluated to determine the most suitable fluid for different applications. Key requirements include compatibility with materials, low viscosity, good thermal conductivity, improved thermal stability, and more. To thoroughly evaluate the environmental impacts and cost considerations of hydrogen and helium, the main findings are summarized in Table 3.

TABLE 3. Cost and economic challenges of fluids [32]

Fluid	Compatible metals			Cost ($/Ltr)	Toxicity	Economic Challenges
	Aluminium	Copper	Stainless Steel			
Hydrogen	√	√	√	1.09 - 3.40	Environmentally Friendly	Infrastructure for safe handling
Helium	√	√	√	10.19 - 20.39	Environmentally Friendly	Limited natural sources

RESULTS

This section investigates the thermal performance and power consumption of BTMS using hydrogen-helium mixtures at various concentrations and flow velocities of 0.5 m/s, 1 m/s, 5 m/s, and 20 m/s. It also assesses the BTMS performance of blending gases against key findings from the literature. Furthermore, it validates the performance of a single transient battery cell by comparing it against both experimental and numerical data. The analysis aims to understand the effects of the blended gases on the maximum temperature, temperature variations, and pressure drops within the BTMS.

HYDROGEN-HELIUM GAS-BASED COOLANT

Effect the Flow velocity of Blended Gases on Thermal Performance

This section discusses the influence of various flow velocities on the thermal performance of BTMS-based immersion cooling. It is significant to explore the effect of flow velocities on BTMS performance due to flow circulation significantly control the battery temperature with the operating conditions. Blended gaseous (hydrogen-helium) with helium concentrations of 40 % are conducted at various velocities of 0.5 m/s, 1 m/s, 5 m/s, and 20 m/s, along with 2C-rate and ambient temperature of 25^{o}C.

The BTMS performance of the 5S1P battery module was assessed by examining the maximum temperature, temperature variation and power consumptions as a key parameter. Figure 3(a) demonstrates the variation in the maximum temperature of the battery cells over time at different coolant velocities. As the coolant velocity increased from 0.5 m/s to 20 m/s, the maximum temperature was decreased from 36.837℃ to 26.456℃, respectively. The reduction in the battery maximum temperature is by approximately 28.181%. It is important to note that increasing the coolant flow rate can significantly enhances the cooling performance of the BTMS by dissipating more heat generated during operation. Therefore, with blended gases at the helium concentration of 40 %, the maximum temperature at various velocities remained within the safety threshold limit ($\leq$ 40℃).

In the immersion cooling system for BTMS, Temperature variation s within the battery cell and across the battery module are unavoidable due to heat dissipation. Significant temperature variations can lead to thermal runaway, which greatly impacts safety, lifespan, and thermal performance. The optimum temperature variation range for battery module is (0 - 5°C) [23, 33]. Figure 3(b) illustrates the temperature variation across the battery module at various inlet velocities. At inlet velocities of 0.5 m/s, 5 m/s, and 20 m/s, the temperature variation within the battery module remained within the safe range ($\leq$ 5.0°C). However, at a low inlet velocity of 0.1 m/s, the Temperature variation exceeded the safety threshold after 470 seconds of discharge, which could potentially trigger thermal runaway.

The relationship between flow velocity and system power consumption is quite notable. As shown in Fig. 4, power consumption rises sharply with increasing flow velocity, climbing from 0.0042 W at 0.5 m/s to 24.611 W at 20 m/s, computed using equation 16. While this significant increase enhances both safety and efficiency, it could adversely impact the energy storage required to power the system. Therefore, the power consumption values of 0.0042 W, 0.0175 W, 0.626 W, and 24.611 W at flow velocities of 0.5 m/s, 1 m/s, 5 m/s, and 20 m/s, respectively, highlight a critical spectrum of thermal management efficiency. The figure of 0.0042W demonstrates inadequate temperature control, resulting in significant variation and alarming potential for thermal runway, as illustrated in Fig. 3b. Conversely, a power consumption of 0.0175 W strikes a commendable balance between optimal thermal performance and safety. Notably, elevated power consumptions rates of 0.626W and 24.611 W indicate excessive energy use which can adversely impact energy storage. Thus, adopting a flow velocity of 1 m/s flow velocity, with a minimum system power consumption of 0.0175 W, emerged as the most effective strategy to acquire reliable numerical data across various gas concentrations.

Figure 5 illustrates the temperature distribution in a 5S1P battery module using blended gaseous with a helium concentration of 40% at a 2C discharge rate. The first three cells exhibit a smaller temperature variation compared to the last two cells due to the specific module configuration employed in this study. The greatest Temperature variations were noted in cells 4 and 5, as the flow of gas absorbs heat from the preceding cells. In battery modules with different configurations (such as other 5S1P arrangements) or with a larger number of cells, the temperature gradients are likely to vary considerably. These variations in temperature are primarily influenced by the module configuration, flow directions, and progressive heating of the fluid. Consequently, the module configuration plays a crucial role in determining cell temperature gradients, underscoring its importance in the design and optimization of battery systems.

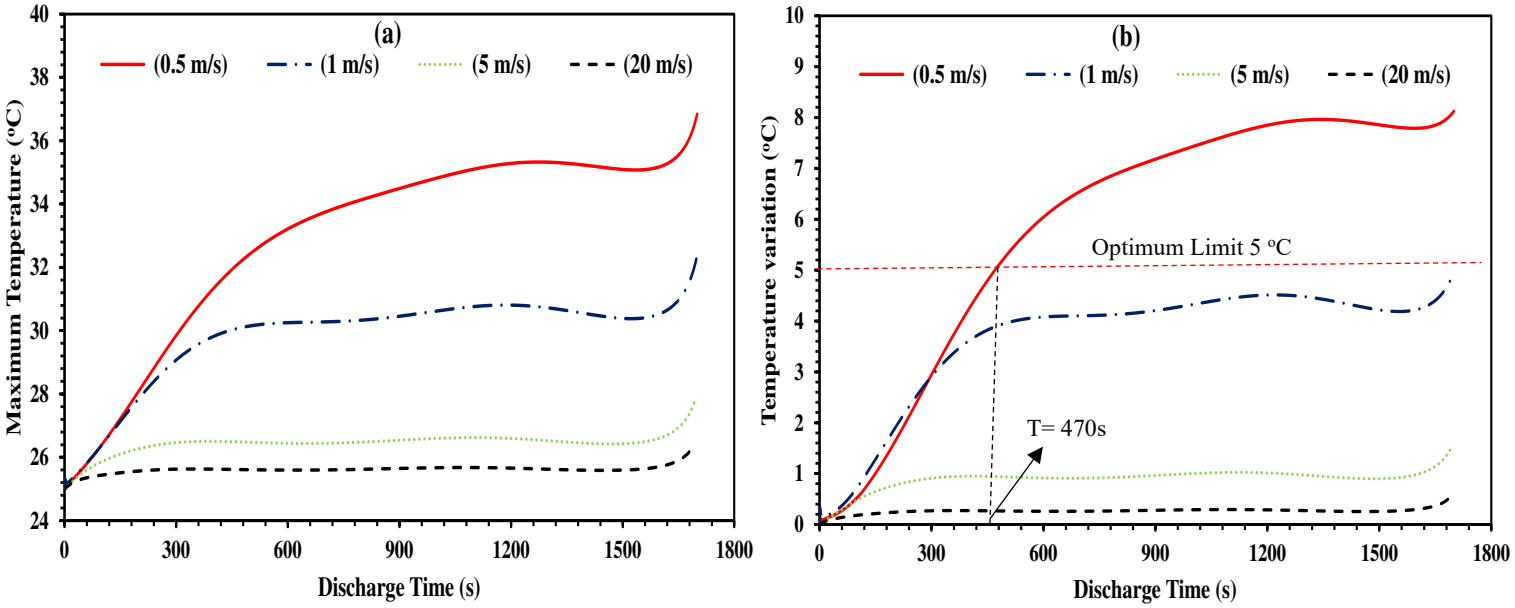

FIGURE 3. Thermal performance of BTMS at helium concentration (0.4) and various flow velocities (0.5 m/s, 1 m/s, 5 m/s &20 m/s): (a) Maximum temperature, (b) Temperature variation.

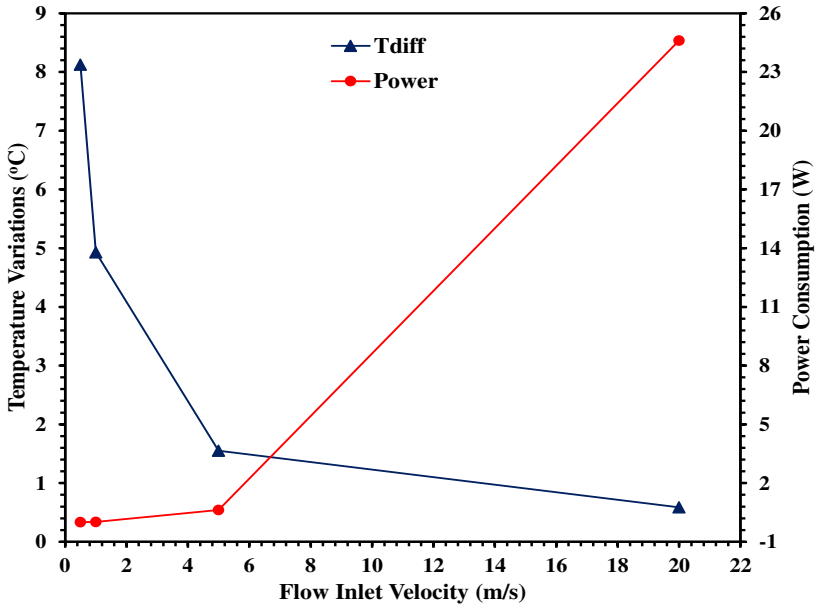

FIGURE 4. System power consumption and Temperature variation at different velocities.

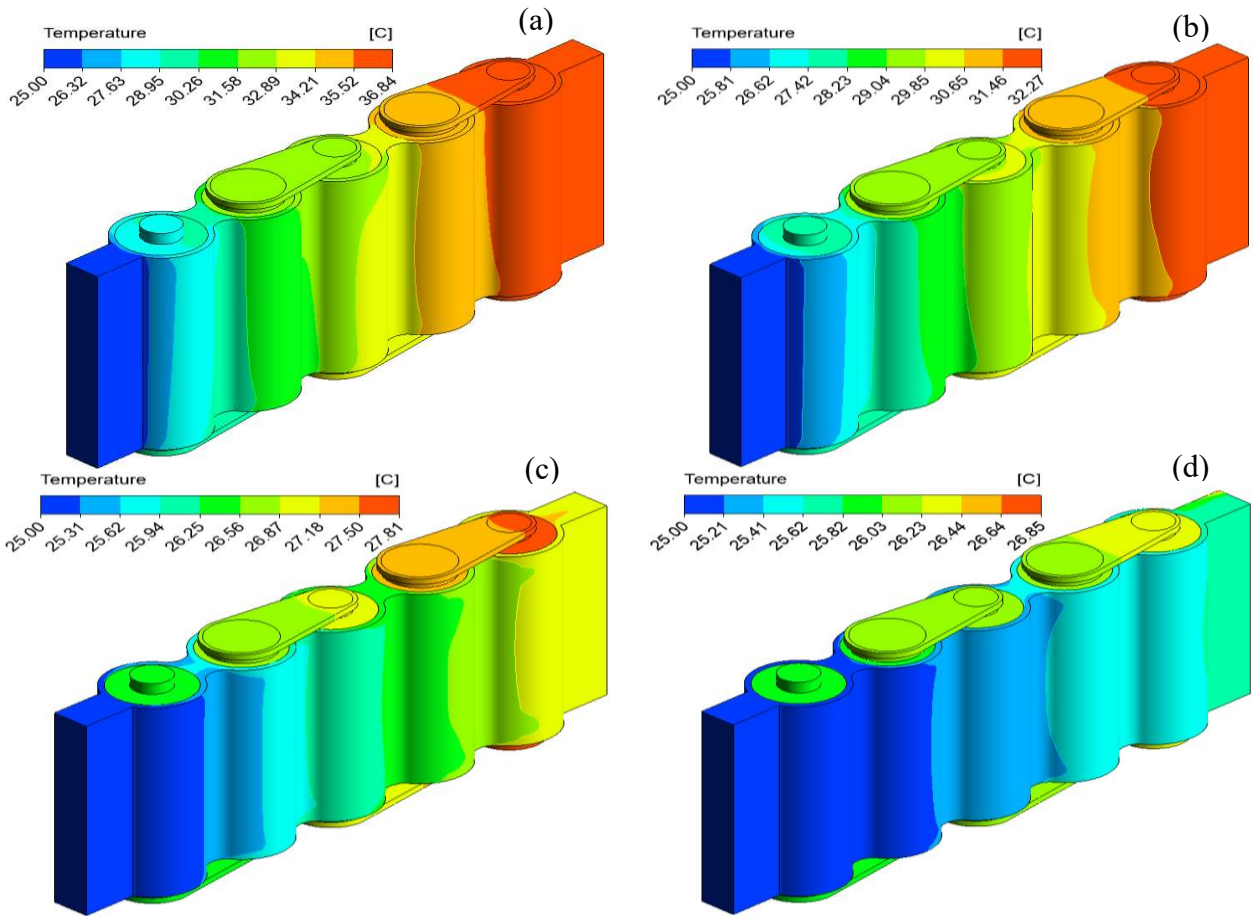

FIGURE 5. Battery module temperature distribution at various flow velocities, (a) 0.5 m/s, (b) 1 m/s, (c) 5 m/s, and (d) 20 m/s.

Effect of Gaseous Blending on Immersion Cooling

This section presents the numerical data of blended gases at a flow velocity of 1 m/s, focusing on various helium concentrations (10%, 20%, 30%, 40%) blended with hydrogen as the primary fluid.

Figure 6 illustrates the maximum temperature and temperature distribution of the battery module (5S1P) at a 2C rate with different gas blends. These results demonstrate how the concentration of blended gaseous influences the battery's thermal performance. Specifically, at helium mixture concentrations of 0.1, 0.2, 0.3, and 0.4, the temperatures rise slightly to about 31.804°C, 31.934°C, 32.123°C, and 32.269°C, respectively. Additionally, the Temperature variation s increased to 4.617°C, 4.711°C, 4.827°C, and 4.931°C for the corresponding mixtures. Importantly, throughout all hydrogen-helium mixtures, both the maximum temperature and the temperature variation remain within the safe operational range, affirming the reliability of these blends for optimal battery performance.

Interestingly, a helium concentration of 10% showed slightly better cooling performance compared to a 40% concentration. The maximum temperature and temperature variation increased by 1.462% and 6.8%, respectively, at 0.4 helium blended. This observation can primarily be attributed to the increased density of the gas mixture, which results in higher frictional losses and flow resistance. Nevertheless, using a hydrogen-helium blend at a 40% concentration is highly recommended to reduce the flammability of hydrogen by increasing its ignition threshold. Despite these challenges, all tested scenarios succeeded in keeping the maximum temperature and temperature variation of the battery module below the safety threshold of 40°C.

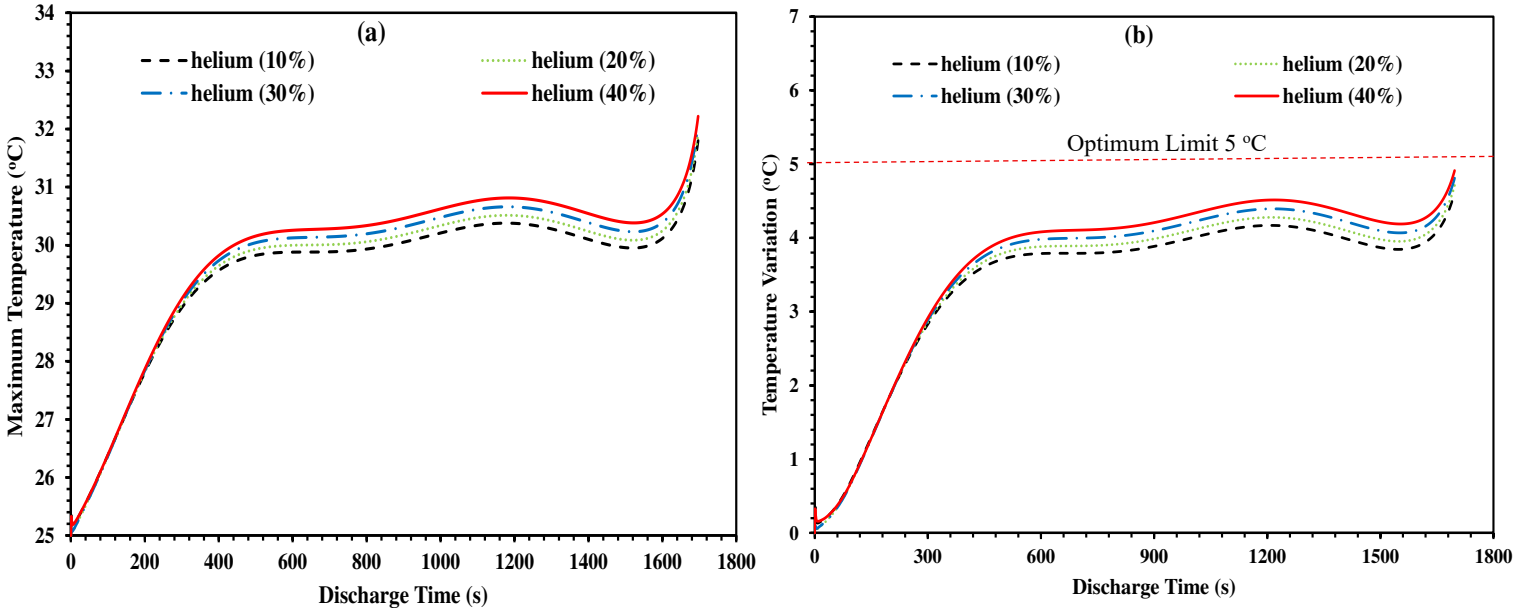

FIGURE 6. Temperature variation at various gases concentrations and flow velocities (a) 0.5 m/s, (b) 1 m/s, and (c) 5 m/s.

Comparative Analysis of Gas Blends with Experimental Work

A hydrogen-helium blend at a 40% concentration demonstrated superior cooling performance compared to air cooling, thermal oil cooling, and mineral oil cooling. The use of a helium mixture at this concentration significantly reduced the flammability of hydrogen gas, making the blended gases well-suited for BTMS applications.

To thoroughly understand and evaluate the current numerical study, qualitative comparisons were made with experimental work that utilized air, thermal oil, and mineral oil-based cooling to validate the key thermal performance indicators, specifically the maximum temperature, as referenced in [34]. The experimental study was conducted on 20 cylindrical cells with a nominal capacity of 10 Ah, using a forced air-cooling inlet velocity of 4 m/s and a mass flow rate of 0.02 kg/s for both types of oil cooling. The design of BTMS employed in the experimental work differs from that of the current BTMS design. The experimental setup is designed as a rectangular enclosure with dimensions of 120 (L) x 115 (W) x 90 (H) mm to accommodate the cylindrical batteries. Thus, the maximum temperatures observed at a 2C rate for air, thermal oil, and mineral oil immersion cooling were 38 °C, 34 °C, and 33 °C, respectively. In contrast, the current study using hydrogen-helium as a coolant reduced the maximum temperatures by 15%, 5%, and 2.2% compared to air, thermal oil, and mineral oil cooling, respectively, as shown in Fig. 7.

As a result, the maximum temperature of the LIB module (5S1P) at a 2C rate and 1 m/s flow rate was recorded at 32.3 °C. Thus, utilizing a helium-blended gas at a 40% concentration effectively kept the BTMS within safe operating limits while achieving superior cooling compared to the experimental methods.

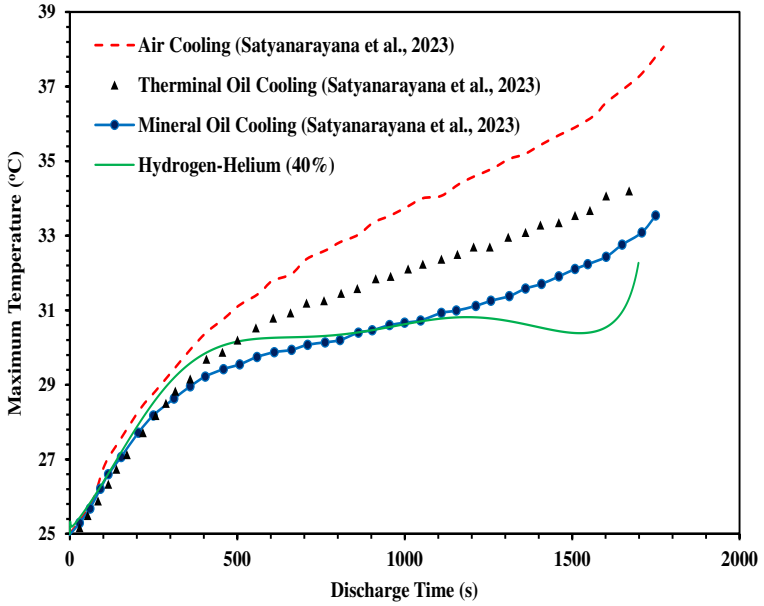

FIGURE 7. 5S1P maximum temperature of battery module comparison with immersion cooling [34] at 2C-rate.

In addition, another qualitative study was conducted featuring experimental work that used helium-based immersion cooling system to assess the thermal performance of a BTMS using hydrogen-helium. The experimental study involved a pouch battery cell, each with a nominal capacity of 20 Ah $LiFePO_4$ (LFP), and employed helium gas as a cooling medium, as referenced in [35]. The battery cell was placed in a sealed container measuring 310 x 200 x 40 mm, with the inlets and outlets having a diameter of 1/8 inch positioned on opposite faces of the container. During the experiments, the recorded temperature reached 16.2 °C at a 3C discharge rate. In contrast, the current study achieved a temperature of 12.721 °C under the same discharge current. This represents a temperature reduction of 21.475% when using hydrogen-helium as a coolant compared to the helium coolant, as illustrated in Fig. 8. Therefore, the strategic use of a helium-blended gas at a 40% concentration effectively maintained the BTMS within safe operating limits while providing superior cooling performance.

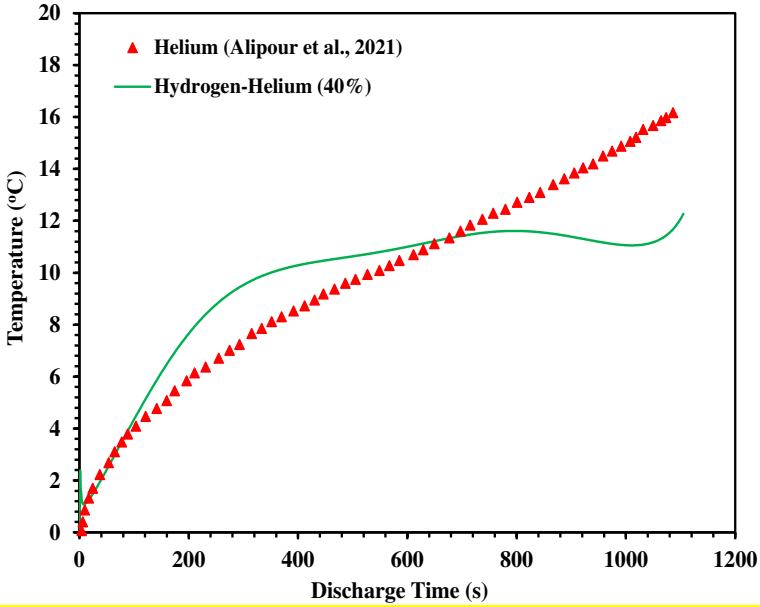

FIGURE 8. 5S1P maximum temperature of battery module comparison with helium gas [35] at 3C-rate.

Validation of Numerical Model

The performance of the 3D-transient cylindrical battery cell has been validated against both experimental and numerical data from Donmez et al. [18]. The thermal performance of the battery was assessed with a nominal cell capacity of 6 Ah, at a 3C discharge rate and an initial temperature of 300K. The results indicate that the numerical data is accurate and aligns well with both the experimental and numerical findings, as shown in Fig. 9. Thus, the thermal behavior of the cylindrical cell is considered appropriate for this study.

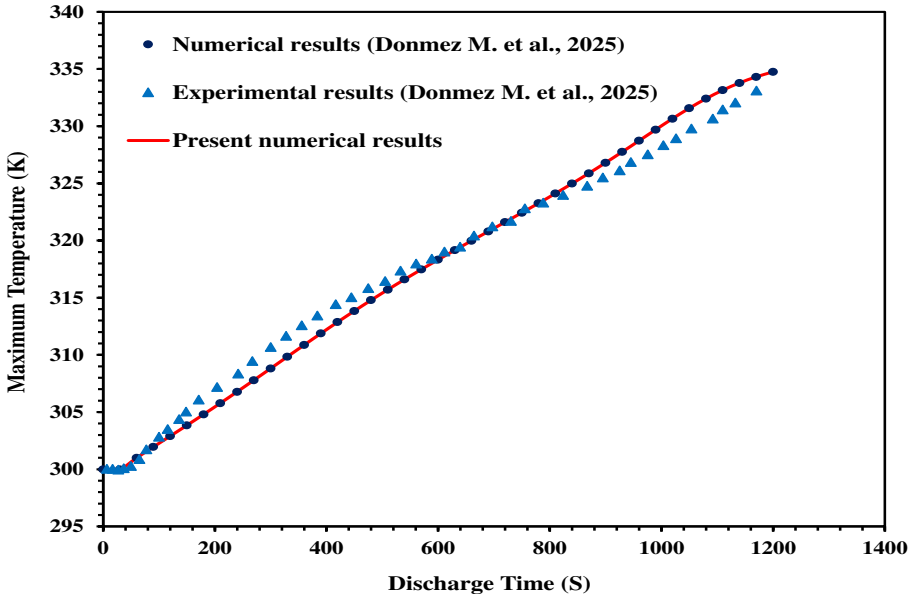

FIGURE 9. Numerical validation against experimental numerical results [18].

CONCLUSION

This study investigates the thermal performance and power consumption of a novel BTMS for 5S1P LIB module, based on immersion cooling using hydrogen-helium gas blends. The effects of flow velocities (0.5 - 20 m/s) and helium concentrations (10% - 40%) were analyzed at 2C discharge rate. The key findings are as follows:

- Higher coolant velocities significantly improve cooling performance, reducing the maximum battery temperature. However, this comes with a substantial increase in system pumping power consumption. A velocity of 1 m/s was identified as an optimal trade-off, maintaining safe temperatures ($T_{max} < 40°C$, $T_{diff} < 5°C$) with minimal power draw (0.0175 W). A very low velocity (0.5 m/s) led to an unsafe Temperature variation (>5°C).
- Increasing the helium concentration from 10% to 40% slightly elevates the maximum temperature and temperature variation due to increased gas mixture density, which amplifies frictional losses and flow resistance. However, all blends successfully maintained temperatures within safe operational limits. The safety benefit of drastically reduced hydrogen flammability with a 40% He blend far outweighs the minor performance penalty.
- A comparative analysis demonstrated that the hydrogen-helium blend (40% He) outperforms traditional cooling methods. It reduced the maximum operating temperature by 15%, 5%, and 2.2% compared to air cooling, thermal oil immersion, and mineral oil immersion, respectively. Furthermore, it decreased the battery temperature by 21.475% compared to helium-based coolant.

In summary, the findings confirm the significant potential of the investigated hydrogen-helium BTMS proposal to enhance cooling efficiency and safety in various applications, paving the way for advancements in other thermal management technologies.

ACKNOWLEDGMENTS

This research was funded by the Higher Committee for Education Development in Iraq (HCED) under contract No. D23431. It was also supported by the University of Leeds and the University of Fallujah.

REFERENCES

[1] Y. Li *et al.*, "Experimental investigations of liquid immersion cooling for 18650 lithium-ion battery pack under fast charging conditions," *Appl Therm Eng*, vol. 227, Jun. 2023, doi: 10.1016/j.applthermaleng.2023.120287.

[2] P. Ahmadi, "Environmental impacts and behavioral drivers of deep decarbonization for transportation through electric vehicles," *J Clean Prod*, vol. 225, pp. 1209–1219, Jul. 2019, doi: 10.1016/j.jclepro.2019.03.334.

[3] M. Al Qubeissi, A. Almshahy, A. Mahmoud, M. T. Al-Asadi, and R. M. A. Shah, "Modelling of battery thermal management: A new concept of cooling using fuel," *Fuel*, vol. 310, 2022, doi: 10.1016/j.fuel.2021.122403.

[4] Y. Liu, G. Aldan, X. Huang, and M. Hao, "Single-phase static immersion cooling for cylindrical lithium-ion battery module," *Appl Therm Eng*, vol. 233, Oct. 2023, doi: 10.1016/j.applthermaleng.2023.121184.

[5] M. Al Qubeissi *et al.*, "Comparative Analysis of Battery Thermal Management System Using Biodiesel Fuels," *Energies (Basel)*, vol. 16, no. 1, 2023, doi: 10.3390/en16010565.

[6] A. Wahab, A. U. H. Najmi, H. Senobar, N. Amjady, H. Kemper, and H. Khayyam, "Immersion cooling innovations and critical hurdles in Li-ion battery cooling for future electric vehicles," Apr. 01, 2025, *Elsevier Ltd*. doi: 10.1016/j.rser.2024.115268.

[7] A. R. Abdulmunem, H. M. Hamed, P. M. Samin, I. I. Mazali, and K. Sopian, "Thermal management of lithium-ion batteries using palm fatty acid distillate as a sustainable bio-phase changes material," *J Energy Storage*, vol. 73, pp. 109–187, Oct. 2023, doi: https://doi.org/10.1016/j.est.2023.109187.

[8] Y. Liu and J. Zhang, "Self-adapting J-type air-based battery thermal management system via model predictive control," *Appl Energy*, vol. 263, Apr. 2020, doi: 10.1016/j.apenergy.2020.114640.

[9] P. Qin, M. Liao, D. Zhang, Y. Liu, J. Sun, and Q. Wang, "Experimental and numerical study on a novel hybrid battery thermal management system integrated forced-air convection and phase change material," *Energy Convers Manag*, vol. 195, pp. 1371–1381, Sep. 2019, doi: 10.1016/j.enconman.2019.05.084.

[10] C. Roe *et al.*, "Immersion cooling for lithium-ion batteries – A review," Mar. 30, 2022, *Elsevier B.V.* doi: 10.1016/j.jpowsour.2022.231094.

[11] W. Wu, S. Wang, W. Wu, K. Chen, S. Hong, and Y. Lai, "A critical review of battery thermal performance and liquid based battery thermal management," Jan. 01, 2019, *Elsevier Ltd*. doi: 10.1016/j.enconman.2018.12.051.

[12] H. Hu, J. Xu, J. Li, and H. Xi, "Immersion coupled direct cooling with non-uniform cooling pipes for efficient lithium-ion battery thermal management," *J Energy Storage*, vol. 116, Apr. 2025, doi: 10.1016/j.est.2025.116010.

[13] M. Al Qubeissi, R. M. R. A. Shah, and A. Almshahy, "Battery thermal management using heavy fuels: An approach to lightweight diesel fuelled hybrid electric vehicles," *Alexandria Engineering Journal*, vol. 126, pp. 515–545, Jul. 2025, doi: 10.1016/j.aej.2025.04.064.

[14] L. Barelli *et al.*, "Oxygen reduction approaches for fire protection to increase grid Li-ion BESS safety," in *E3S Web of Conferences*, EDP Sciences, Feb. 2021. doi: 10.1051/e3sconf/202123809001.

[15] M. Al-Zareer, I. Dincer, and M. A. Rosen, "Performance assessment of a new hydrogen cooled prismatic battery pack," *Energy Convers Manag*, vol. 173, pp. 303–319, Aug. 2018, doi: https://doi.org/10.1016/j.enconman.2018.07.072.

[16] M. A. Rosen and S. Koohi-Fayegh, "The prospects for hydrogen as an energy carrier: an overview of hydrogen energy and hydrogen energy systems," Feb. 01, 2016, *Joint Center on Global Change and*

Earth System Science of the University of Maryland and Beijing Normal University. doi: 10.1007/s40974-016-0005-z.

[17] K. Shivaprasad, S. Raviteja, P. Chitragar, and G. N. Kumar, "Experimental Investigation of the Effect of Hydrogen Addition," *Procedia Technology*, vol. 14, pp. 141–148, Sep. 2024, doi: https://doi.org/10.1016/j.protcy.2014.08.019.

[18] Qiu, L.; Wang, K.; Ma, Y. Proceedings of the 28th International Cryogenic Engineering Conference and International Cryogenic Materials Conference 2022: ICEC28-ICMC 2022, Hangzhou, China; Springer Nature, 2023; Vol. 70.

[19] M. Donmez, M. Tekin, and M. I. Karamangil, "Artificial neural network predictions for temperature Utilizing numerical anaylsis in immersion cooling system using mineral oil and an engineered fluid for 32700," *International Journal of Thermal Sciences*, vol. 211, pp. 109–742, Jan. 2025, doi: https://doi.org/10.1016/j.ijthermalsci.2025.109742.

[20] Y. Zhang *et al.*, "Performance comparison between straight channel cold plate and inclined channel cold plate for thermal management of a prismatic LiFePO4 battery," *Energy*, vol. 248, Jun. 2022, doi: 10.1016/j.energy.2022.123637.

[21] G.-H. Kim, K. Smith, K.-J. Lee, S. Santhanagopalan, and A. Pesaran, "Multi-Domain Modeling of Lithium-Ion Batteries Encompassing Multi-Physics in Varied Length Scales," *J Electrochem Soc*, vol. 158, no. 8, p. A955, 2011, doi: 10.1149/1.3597614.

[22] K. H. Kwon, C. B. Shin, T. H. Kang, and C.-S. Kim, "A two-dimensional modeling of a lithium-polymer battery," *J Power Sources*, vol. 163, pp. 151–157, Apr. 2006.

[23] M. S. Patil, J.-H. Seo, and M.-Y. Lee, "A novel dielectric fluid immersion cooling technology for Li-ion battery thermal managment," *Energy Convers Manag*, vol. 229, p. 113, Dec. 2021.

[24] M. K. Tran, A. Mevawala, S. Panchal, K. Raahemifar, M. Fowler, and R. Fraser, "Effect of integrating the hysteresis component to the equivalent circuit model of Lithium-ion battery for dynamic and non-dynamic applications," *J Energy Storage*, vol. 32, Dec. 2020, doi: 10.1016/j.est.2020.101785.

[25] M. Zamani, S. Seddighi, and H. R. Nazif, "Erosion of natural gas elbows due to rotating particles in turbulent gas-solid flow," *J Nat Gas Sci Eng*, vol. 40, pp. 91–113, Feb. 2017, doi: https://doi.org/10.1016/j.jngse.2017.01.034.

[26] R. Banerjee and K. Nidhul, "Effect of various dielectric fluids on temperature homogeneity of Li-ion battery pack in an energy efficient novel immersion cooling design," *Results in Engineering*, vol. 26, Jun. 2025, doi: 10.1016/j.rineng.2025.104688.

[27] H. Wang, T. Tao, J. Xu, H. Shi, X. Mei, and P. Gou, "Thermal performance of a liquid-immersed battery thermal management system for li-ion pouch batteries," *J Energy Storage*, vol. 46, p. 103, Dec. 2022, doi: https://doi.org/10.1016/j.est.2021.103835.

[28] A. G. Olabi *et al.*, "Large-vscale hydrogen production and storage technologies: Current status and future directions," *Int J Hydrogen Energy*, vol. 46, no. 45, pp. 23498–23528, Jul. 2021, doi: 10.1016/j.ijhydene.2020.10.110.

[29] T. Sinigaglia, F. Lewiski, M. E. S. Martins, and J. C. M. Siluk, "Production, storage, fuel stations of hydrogen and its utilization in automotive applications-a review," *Int J Hydrogen Energy*, vol. 42, no. 39, pp. 24597–24611, Sep. 2017, doi: https://doi.org/10.1016/j.ijhydene.2017.08.063.

[30] B. Abderezzak, K. Busawon, and R. Binns, "Flows consumption assessment study for fuel cell vehicles: Towards a popularization of FCVs technology," *Int J Hydrogen Energy*, vol. 42, no. 17, pp. 12905–12911, Apr. 2017, doi: 10.1016/j.ijhydene.2016.12.152.

[31] Y. Sun, J. Ogden, and M. Delucchi, "Societal lifetime cost of hydrogen fuel cell vehicles," *Int J Hydrogen Energy*, vol. 35, no. 21, pp. 11932–11946, Nov. 2010, doi: 10.1016/j.ijhydene.2010.08.044.

[32] R. Kumar and V. Goel, “A study on thermal management system of lithium-ion batteries for electrical vehicles: A critical review,” Nov. 01, 2023, *Elsevier Ltd*. doi: 10.1016/j.est.2023.108025.

[33] A. Almshahy, Z. Khatir, K. J. Kubiak, and M. Al Qubeissi, “Framework for rapid design and optimisation of immersive battery cooling system,” Jul. 07, 2025. doi: 10.21203/rs.3.rs-6991924/v1.

[34] G. Satyanarayana, D. Ruben Sudhakar, V. Muthya Goud, J. Ramesh, and G. A. Pathanjali, “Experimental investigation and comparative analysis of immersion cooling of lithium-ion batteries using mineral and therminol oil,” *Appl Therm Eng*, vol. 225, May 2023, doi: 10.1016/j.applthermaleng.2023.120187.

[35] M. Alipour, A. Hassanpouryouzband, and R. Kizilel, “Investigation of the Applicability of Helium-Based Cooling System for Li-Ion Batteries,” *Electrochem*, vol. 2, no. 1, pp. 135–148, Mar. 2021, doi: 10.3390/electrochem2010011.